Scaling properties of diffusion-limited aggregation, the percolation hull, and invasion percolation

Stefan Schwarzer,[1] Shlomo Havlin,[1,2] and H. Eugene Stanley[1]
[1] *Center for Polymer Studies and Department of Physics, Boston University, Boston, Massachusetts 02215*
[2] *Department of Physics, Bar-Ilan University, Ramat-Gan, Israel*
(Received 12 October 1992; revised manuscript received 11 October 1993)

We study various properties of the surface of diffusion-limited aggregation (DLA) and invasion percolation clusters using a "glove algorithm." Specifically, we define the ℓ-perimeter to be the set of nonfractal sites with a chemical distance ℓ from a fractal with M sites. We argue that $P(M,\ell)$, the number of sites of the ℓ-perimeter, should obey a scaling law of the form $P(M,\ell)/\ell \sim f(\ell/M^{1/d_f})$, where $f(u) \sim u^{-d_f}$ for $u \to 0$ and $f(u) \to$ const for $u \to \infty$. Simulations of two-dimensional off-lattice DLA clusters, invasion percolation clusters, and percolation hulls—as well as an exact treatment of the Sierpiński gasket—support this scaling form. We find that an analogous scaling form holds for $G(M,\ell)$, the number of sites in the "ℓ-glove," which is composed of the sites of the ℓ-perimeter accessible to particles of radius ℓ from the exterior. Moreover, we define a hierarchy of "lagoons" for the case of loopless fractals as regions that are inaccessible to particles of different sizes. We apply this definition to DLA and find that the lagoon-size distribution in DLA is consistent with a self-similar structure of the aggregate. However, we find even for large lagoons a surprisingly small most probable width of the necks that separate the lagoons from the exterior of the cluster. Small neck widths of large lagoons are consistent with a recently proposed void-neck model for the geometric structure of DLA.

PACS number(s): 05.40.+j, 61.50.Cj, 64.60.Ak, 81.10.Jt

I. INTRODUCTION

Unlike the points of a compact object, a large fraction of the sites of a fractal are "exposed" to points that do not belong to the fractal itself. In other words, a fractal is almost entirely composed of "surface" [1]. This observation explains why fractals are of great importance in a wide range of disciplines. In biology, matter exchange takes place across membranes and often requires large contact areas of the participating systems: oxygen diffuses into the blood in lung tissue and trees absorb nutrients through their widely branched root network. In chemistry, reaction rates depend on the surfaces that the reacting species expose to one another. The surface of a catalyst plays a central role in catalytically controlled reactions. The use of porous media as electrodes for batteries [2,3] is also important for applications.

In particular, the present study addresses surface properties of diffusion-limited aggregation (DLA) [3–9], invasion percolation (IP) [10,11], and percolation hull (PH) [12] clusters. In the DLA model a seed particle is placed in the center of a coordinate system and a random walk is released from "infinity." On contact, the walker sticks to the growing aggregate, whereupon a new particle is released. This procedure is repeated until an aggregate of the desired size is formed. As the cluster grows, its interior is increasingly screened from the exterior, because incoming particles are more likely to stick to the tips of the aggregate. A complex, branched, random fractal is formed, which displays rich scaling properties [13–17] that are still not fully understood [18]. To improve the simple structural models of DLA [19–21], a better understanding of the geometry of DLA is required. In particular, the importance of "almost closed loops" in the structure of the aggregate is debated in conjunction with highly screened sites [22–25] in parts of the cluster [26]. Since DLA grows by addition of particles approaching from infinity, only the "exterior" (accessible) cluster surface supports growth and its characterization merits attention.

Similar to the DLA case, IP clusters also only grow on their "external" surface [10]. As DLA, IP is also used as a model for fluid displacement in a random medium. The medium is modeled by a lattice occupied with random numbers of uniform distribution. The invasion process starts on a central seed site [10,11,27] and continues by always replacing the smallest accessible random number on the surface of the invasion front by a new IP cluster site. If the invasion process forms a loop such that "defender" fluid is trapped, no more invasion into the trapped region takes place. Two-dimensional (2D) IP clusters have been found to be fractals with dimension of about $d_f^{\mathrm{IP}} \approx 1.82$ [10,11].

Motivated by these two examples, we develop an algorithm — the "glove" algorithm — to measure the following quantities, defined in Sec. II.

(i) The total perimeter of a fractal [cf. Fig. 1(a)], the set of all nearest-neighbor sites of the fractal, and a generalization thereof (ℓ-perimeter) to neighboring sites of higher order. For DLA, IP, and PH we find scaling relations which also suggest a method for the determination of the fractal dimension of an object.

(ii) The accessible perimeter of a fractal [cf. Fig. 1(a)], which is the set of the perimeter sites that can

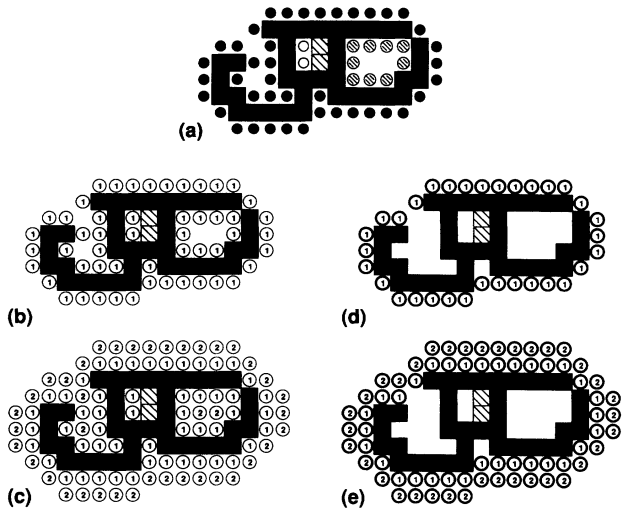

FIG. 1. This figure is designed to illustrate the definitions used throughout the text for the various types of cluster and perimeter sites. We denote the 39 cluster sites by square symbols, the subset of 37 cluster sites that belong to the hull by filled squares, and the remaining two internal cluster sites by hatched squares. (a) The perimeter sites which are nearest neighbors to cluster sites fall into three categories, (i) internal perimeter sites, shown as open circles, (ii) external perimeter sites that are accessible from the exterior only if one can walk on second neighbors, shown as hatched circles, and (iii) the remaining external perimeter sites, called accessible perimeter and shown as filled circles. (b) The 1-perimeter of the same object is the set of *all* nearest-neighbor sites, denoted by the symbol ①. (c) The second step in the construction of the ℓ-perimeter. The 2-perimeter sites are nearest-neighbor sites to the 1-perimeter and denoted by ②. (d) 1-glove (boldface ②). Only 1-perimeter sites that are nearest neighbors to vacant external sites constitute the 1-glove. (e) Empty accessible nearest-neighbor sites of the 1-glove form the 2-glove.

be reached from the exterior of the object, and a generalization thereof (ℓ-gloves) to neighbor sites of higher order. The accessible perimeter has been studied experimentally, e.g., for porous media and fresh fractures [3,28], and theoretically for percolation clusters [29–32]. For the ℓ-gloves of DLA, IP, and PH we find scaling relations similar to those describing the ℓ-perimeter.

(iii) The "lagoon"-size distribution, where "lagoons" are generalizations of the notion of voids to the case of *loopless* fractals [Sec. IV A]. Lagoons are the regions of a fractal which are inaccessible to probe particles with a given size [33]. They are important in connected objects like IP and DLA, where they are delineated by almost closed loops in the geometrical structure.

Our study is organized as follows. First, we introduce the glove algorithm and give precise definitions of the quantities (i) and (ii) in Sec. II. Second, we propose scaling relations for the ℓ-perimeter and the ℓ-gloves which we apply to the case of DLA (Secs. III B 2, III C 2). We analytically calculate the scaling functions for the Sierpiński gasket (Appendix A) and obtain numerical scaling forms for PH (Appendix B) and IP clusters (Appendix C). Third, we define "lagoons" and study their distribution in DLA in detail (Sec. IV). Finally, we summarize our results in Sec. V.

II. THE "GLOVE" ALGORITHM

In this section we present an operational definition of the ℓ-perimeter and the ℓ-glove. For the remainder of this paper, we will assume — as is the case in many computer simulations — that the object studied is specified as a set of discrete points on a square lattice.

A. The ℓ-perimeter

Suppose that we attach a label 0 to all the sites of the investigated object [square-shaped sites in Figs. 1(a)–1(f)]. Here, we follow the notation of Grossman and Aharony [30] introduced for percolation, and use the term "perimeter" to refer to sites that do *not* belong to the object itself [circular sites in Figs. 1(a)–1(e)]. To define the 1-perimeter, we find the nearest-neighbor sites of the object and label them $\ell = 1$, as shown in Fig. 1(b). Similarly, the sites that are nearest neighbors of sites with $\ell = 1$, and not already labeled in the previous step, are identified as $\ell = 2$ sites and form the 2-perimeter [Fig. 1(c)]. We iterate the procedure and thereby label all sites surrounding the object [34]. The number ℓ associated with every lattice site is also called the chemical distance [35] of the site to the object. In general, we will use the term "ℓ-perimeter" to refer to the set of sites with the same label ℓ, and denote their number by $P(M,\ell)$. Here M is the mass or the total number of lattice sites occupied by the object.

B. The ℓ-gloves

Next we describe the procedure to determine the "ℓ-gloves" of the object. In the first step, instead of labeling *all* the neighbor sites of the object as done for the ℓ-perimeter, we place a flexible "glove," one lattice unit thick, on the object.

The 1-glove [boldface symbols ① in Fig. 1(d)] consists of all nearest-neighbor sites of the object which are also nearest neighbors to vacant lattice sites with $\ell = 2$.

To determine the 2-glove, we iterate the process leading to the 1-glove. To this end, we consider the union of the initial fractal and its 1-glove as the object to place the 2-glove on [Figs. 1(d,e)]. We iterate the covering process to obtain ℓ-gloves up to any desired order.

In Fig. 1(d) we display the 1-glove and in Fig. 1(e) the 2-glove for a small object. The ℓ-glove is always a subset of the ℓ-perimeter and as the ℓ-perimeter, the subsequent gloves explore fewer and fewer details of the surface of the object. For large ℓ, greater than half the diameter of the largest "lagoon" (see below), the ℓ-perimeter and the ℓ-glove become identical. We denote the number of sites in the ℓ-glove as $G(M,\ell)$.

C. Related notions and possible generalizations

Before continuing, we remark on related mathematical work. There exist continuum quantities to which ℓ-perimeter and ℓ-glove are closely related. For example, a useful quantity, which can also be successfully employed to determine fractal dimensions, is the Minkowski sausage. The Minkowski sausage, or r-neighborhood of an object, is the set of all points $\mathbf{x}$ with distance $\leq r$ to the object (for mathematically oriented work introducing novel methods to determine the fractal dimension of curves and profiles, see, e.g., [36,37]; for application of the Minkowski sausage concept in physics and chemistry, see, e.g., [38]).

If we replace the Euclidean distance in the continuum by the chemical distance on the lattice and consider ($r = \ell$)-neighborhoods of the fractal on the lattice, then these ℓ-neighborhoods can be regarded as the lattice versions of the Minkowski sausages. The ℓ-neighborhood is the union of ℓ'-perimeters with $\ell' \leq \ell$. Similarly, one can construct the ℓ-neighborhoods by "dilation" of the fractal with a diamond-shaped "structure element" [39]. That is one places a diamond-shaped object of "diameter" $2\ell+1$ on all lattice sites occupied by the fractal and forms the union of all sites covered by this structure element.

Apparently, the $\ell+1$ and the ℓ-neighborhoods differ by the sites occupied by the $(\ell+1)$-perimeter. We note that only the *external* sites of the $(\ell+1)$-perimeter constitute the $\ell+1$-glove. For further illustration, we analytically calculate the Minkowski sausage and continuum analogues of the ℓ-perimeter and ℓ-glove for the Sierpiński gasket in Appendix A.

The numbers ℓ assigned to the sites of a square lattice by the glove algorithm constitute a distance transform of the set of lattice sites occupied by the fractal. A distance transform is an array of numbers representing the shortest distances to occupied lattice sites in a particular metric. In this context, the glove algorithm can be classified as the 4-neighbor distance transform [40]. More sophisticated transforms approximate Euclidean distances more closely and have been used, e.g., in [36] to determine Minkowski sausages. Although we have defined ℓ-glove and ℓ-perimeter for two dimensions, these could be generalized to higher dimensions, as done for the ℓ-perimeter, e.g., in [40].

III. SCALING LAWS FOR PERIMETERS AND GLOVES

A. General remarks

Scaling arguments have successfully been applied in physics to describe a host of phenomena in a variety of fields, most notably critical phenomena. The shortest route to scaling makes use of properties of generalized homogeneous functions [41]. A generalized homogeneous function $f(x,y)$ of two variables x and y obeys the relation

$$f(\lambda^a x, \lambda^b y) = \lambda f(x,y). \tag{3.1}$$

Elementary considerations [41] show that (3.1) is equivalent to writing

$$F(x,y) = y^{1/a} F(x/y^{a/b}, 1) \equiv y^{1/a} f(x/y^{a/b}). \tag{3.2}$$

Here $f(u)$ is called the scaling function and $u \equiv x/y^{a/b}$ the scaling variable. The functional *form* of the scaling function $f(x/y^{a/b})$ and the exponents a and b in this relation are universal, i.e., they are not sensitive to model "details," such as the lattice on which a specific model is studied. Model-dependent "details" enter the *amplitude* of the scaling function.

The rather strong assumption that the studied quantity $F(x,y)$ is a homogeneous function can in general only be justified *a posteriori*, by the empirical success in extracting invariant, universal features from data sets.

In the following sections, we will discuss scaling relations of the above form for the ℓ-perimeter and the ℓ-glove of DLA, PH, and IP. To this end, we will assume that the scaling variable is an appropriate combination of the chemical distance ℓ and the number M of occupied lattice sites. We relate the exponents of the encountered scaling relations to known exponents of these models, in particular, the fractal dimension of the object itself and the fractal dimension of its external perimeter, respectively. Moreover, some features of the functional form of the scaling functions will be explained.

B. Scaling of the ℓ-perimeter $P(M,\ell)$

1. *Scaling arguments*

We first analyze the ℓ-perimeter in detail and derive a scaling form for the behavior of $P(M,\ell)$.

For small but fixed values of ℓ (much smaller than a crossover value $\ell_\times$ on the order of the linear extension of the cluster), we expect that $P(M,\ell)$ is asymptotically proportional to M [42],

$$P(M,\ell) \sim b(\ell) M \qquad [\ell \ll \ell_\times(M)]. \tag{3.3a}$$

To study the ℓ dependence of $b(\ell)$, we note that if ℓ increases, $P(M,\ell)$ will initially decrease due to the smoothening process as the ragged perimeter of the fractal is successively filled in [Figs. 1(b,c)]. We next argue that the fractal dimension d_f characterizes this smoothening process. If we cover the fractal by boxes of linear size ϵ, then the number of boxes containing points of the fractal is $N(\epsilon) \sim \epsilon^{-d_f}$. The perimeter of the boxes is an approximation to the $\ell(=\epsilon/2)$-perimeter of the fractal. Thus, for fixed M, $P(M,\ell)$ is proportional to $N(2\ell)\ell \sim \ell^{-d_f+1}$; so we expect

$$b(\ell) \sim \ell^{-d_f+1} \qquad [\ell \ll \ell_\times(M)]. \tag{3.3b}$$

For $\ell \gg \ell_\times(M)$ details of the cluster structure are no longer important. Since voids in fractals occur on all length scales, up to the size of the fractal, we expect $\ell_\times(M)$ to be of the size of the linear extension of the fractal. Thus, for large ℓ, the ℓ-perimeter behaves like the perimeter of a nonfractal object,

$$P(M,\ell) \sim \ell \qquad [\ell \gg \ell_\times(M)]. \tag{3.3c}$$

The relations (3.3a)–(3.3c) can be cast into a single scaling form [cf. Eq. (3.2)],

$$P(M,\ell) \sim \ell^\alpha f(u), \quad u \equiv \ell/M^\beta, \tag{3.4}$$

where the scaling function $f(u)$ and the exponents α, β are constrained by Eqs. (3.3a)–(3.3c) The exponents α and β are determined as follows. (i) Since for large values of u, when $\ell \gg \ell_\times(M)$, $P(M,\ell)$ does not depend on M, we expect that $f(u)$ approaches a constant. Comparison of Eq. (3.4) with (3.3c) shows that $\alpha = 1$. (ii) For small arguments, $f(u)$ must display a power-law singularity in order to recover Eqs. (3.3a) and (3.3b). If we assume that $f(u) \sim u^{-\psi}$, then

$$P(M,\ell) \sim \ell^{\alpha-\psi}/M^{-\beta\psi} \tag{3.5}$$

and we obtain $\psi = d_f$ and $\beta = 1/\psi = 1/d_f$. The constant crossover value $u_\times$ between these two regimes is determined by $\ell_\times$;

$$u_\times \equiv \ell_\times(M)/M^{1/d_f}. \tag{3.6}$$

Thus $\ell_\times(M)$ has a power-law dependence on M, $\ell_\times \sim M^{1/d_f}$, and is proportional to the linear extension M^{1/d_f} of the cluster.

Finally, the scaling relation (3.4) takes the form

$$P(M,\ell) \sim \ell f(\ell/M^{1/d_f}), \tag{3.7a}$$

where

$$f(u) \sim \begin{cases} u^{-d_f}, & u \to 0 \\ \text{const}, & u \to \infty. \end{cases} \tag{3.7b}$$

We note that a scaling plot of $f(u)$ as in Fig. 2(a) can be used to determine d_f. The unknown value of d_f should be considered as a parameter that must be adjusted in order to obtain the best possible data collapse. The exponent characterizing $f(u)$ for small u can be used to test the value of d_f. For growth models such as DLA, the scaling of the ℓ-perimeter combines information about the growth dynamics — the increasing linear extension of the cluster as a function of cluster mass — with information about the static structure of a fixed size cluster — here, d_f.

2. *Diffusion-limited aggregation*

We study the ℓ-perimeter of PH and IP as test cases in Appendixes B and C while here we concentrate on the determination of the scaling function $f_{\rm DLA}(u)$ for the ℓ-perimeter of DLA.

Even rather small *on-lattice* DLA is known to display lattice effects that lead to anisotropic cluster growth [43], since growth occurs preferably in the direction of the lattice axes. Consequently, we base our analysis of DLA on clusters grown *off lattice*. The coordinates of 2D off-lattice DLA clusters are discretized such that the cluster is a connected object of nearest- and next-nearest-neighbor lattice sites.

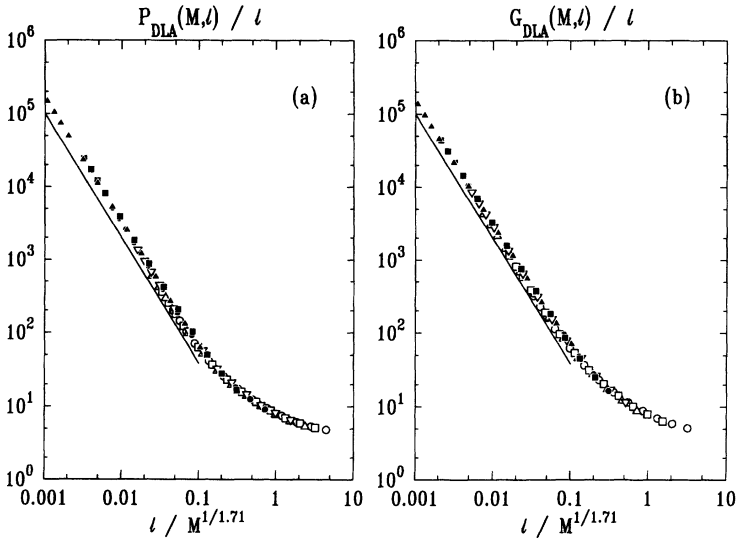

FIG. 2. (a) The scaling function $f_{\rm DLA}(u) \equiv P_{\rm DLA}(M,\ell)/\ell$ vs $u = \ell/M^{1/1.71}$ for the DLA case. M refers to the number of particles in the aggregate, ranging from 50 to 120 000. The data are obtained by averaging over 21 2D off-lattice DLA clusters. The ℓ values are 1 (▲), 3 (■), 7 (•), 15 (△), 23 (▽), 31 (□), and 43 (○). Results obtained for ℓ-perimeters determined using *next-nearest neighbors* are not displayed; however, they differ only in the amplitude of $P_{\rm DLA}(M,\ell)$. (b) $g_{\rm DLA}(u) \equiv G_{\rm DLA}(M,\ell)/\ell$ vs $u = \ell/M^{1/1.71}$ for DLA. The (scheme B) 1-glove is a subset of the 1-surface, the set of nearest-neighbor sites of the cluster, comprising the sites that are still susceptible for further growth. Displayed ℓ-values are 1 (▲), 2 (■), 3 (•), 5 (▽), 7 (△), 15 (□), and 31 (○). The data are averaged over 21 DLA clusters of mass $M = 50, \ldots, 120\,000$. We obtain similar results that only differ in the amplitude of $G_{\rm DLA}(M,\ell)$ if nearest-neighbor connectivity in scheme B is replaced by next-nearest-neighbor (NNN) connectivity or if the ℓ-gloves are calculated as subsets of ℓ-perimeters based on NNN connectivity.

In Fig. 2(a) we display our calculation of the scaling function

$$f_{\mathrm{DLA}}(u) \equiv P_{\mathrm{DLA}}(M,\ell)/\ell \tag{3.8}$$

for DLA, where $u \equiv \ell/M^{1/d_f}$ is the scaling variable. We analyze 21 off-lattice DLA clusters for a sequence of values of M up to 120 000.

For small u, we find straight line behavior of $f_{\mathrm{DLA}}(u)$ with a slope of $\approx 1.73 \pm 0.03$, which is close to the fractal dimension $d_f = 1.715 \pm 0.004$ [44] of DLA as obtained from analyses of the scaling of cluster mass as a function of its radius of gyration. For large u, $f_{\mathrm{DLA}}(u)$ converges towards a constant value [Eq. (3.7b)] equal to 4, as expected for off-lattice DLA discretized on a square lattice.

C. Scaling of the ℓ-glove $G(M,\ell)$

1. *Scaling arguments*

In general, since the ℓ-glove is a subset of the ℓ-perimeter, we know that

$$G(M,\ell) \le P(M,\ell). \tag{3.9}$$

Therefore, if we consider the ℓ-glove and the ℓ-perimeter of a fractal for equal but arbitrary ℓ as fractals in their own right, we obtain the relation $d_{\mathrm{perimeter}} \ge d_{\mathrm{glove}}$, where $d_{\mathrm{perimeter}}$ and d_{glove} are the fractal dimensions of ℓ-perimeter and ℓ-glove for fixed, but arbitrary ℓ. In Sec. III B, we have argued that in fact $d_{\mathrm{perimeter}} = d_f$, independent of ℓ, provided $\ell \ll \ell_\times$.

A similarly strong statement cannot be made for the ℓ-glove. For example, in Appendix B we show that the 1-glove and the 2-glove of percolation have *different* fractal dimensions.

We will ask whether a similar effect, viz., a difference in the fractal dimension of ℓ-perimeter and ℓ-glove for specific ℓ, occurs also in other fractals, e.g., DLA. To this end we will assume that the scaling relations (3.7a) and (3.7b) also hold for the scaling of the length of the ℓ-gloves $G(M,\ell)$,

$$G(M,\ell) \sim \ell g(\ell/M^{1/d_f}), \tag{3.10a}$$

where

$$g(u) \sim \begin{cases} u^{-d_f}, & u \to 0 \\ \text{const}, & u \to \infty. \end{cases} \tag{3.10b}$$

Here, we use the symbol g to denote the scaling functions associated with the ℓ-gloves.

Different fractal dimensions of ℓ-gloves for different ℓ — as in the percolation case — will be heralded by a breakdown of Eqs. (3.10a) and (3.10b).

2. *Diffusion-limited aggregation*

The motivation to study the ℓ-gloves of DLA originates in the quest for a structural model of the cluster structure [20–24,26]. DLA fjords display pronounced sidebranching and as a result of the growth process, two of these branches may approach each other from opposite sides of the fjord to form a "neck." If such neck formation is an essential feature of DLA structure, then it can possibly be detected in the scaling behavior of the ℓ-gloves, since, if ℓ increases, narrow necks are no longer penetrated by the ℓ-glove. As a consequence, for $\ell > 1$, the ℓ-glove may have a smaller fractal dimension than the DLA cluster itself.

The mass dependence of the number of perimeter sites susceptible to further growth in 2D on-lattice DLA, which is *identical* to the 1-glove of the cluster, has been studied in [45] in a different context and found to be proportional to the cluster mass, in agreement with the scaling relations Eqs. (3.10a) and (3.10b). We display a scaling plot [Fig. 2(b)] of

$$g_{\mathrm{DLA}}(u) \equiv G_{\mathrm{DLA}}(M,\ell)/\ell \tag{3.11}$$

for $\ell \ge 1$, where the scaling variable is $u \equiv \ell/M^{1/1.71}$. Here, the exponent 1.71 yields the best data collapse. We find the exponent of the singularity of $g_{\mathrm{DLA}}(u)$ for small u to be 1.73 ± 0.05. Both numbers, 1.71 and 1.73 ± 0.05, agree with the fractal dimension of DLA determined in Sec. III B. The data collapse implies that *all* the ℓ-gloves of DLA, with $\ell \ll \ell_\times(M) \sim M^{1/d_f}$, have the *same* fractal dimension as the cluster itself.

Thus we do not find evidence for a different scaling of narrow necks in the DLA structure from a study of the ℓ-gloves. Also, unlike the percolation models, DLA does not display different fractal dimensions of ℓ-perimeters and ℓ-gloves.

IV. DISTRIBUTION OF LAGOON SIZES AND NECK WIDTHS FOR DLA

Next, we will describe another attempt made to identify effects of neck formation in DLA fjords. We first introduce the notion of "lagoons" to generalize the notion of voids in regular fractals to the case of loopless fractals (or any collection of points).

A. Definition of "necks" and "lagoons"

Consider, e.g., a circle with a small opening of width $w = 2\ell_0$, a simple example of a loopless object [other examples with various openings are given in Figs. 3(a)–3(c)]. Cover the surface with gloves, one after the other. When the number of gloves equals ℓ_0, the glove cannot penetrate into the opening, leaving some interior sites vacant. For a general connected object, after having placed a sufficient number of gloves, we recognize several distinct connected patches of vacant sites isolated from each other by gloves. Each of these patches identifies what we call a "lagoon." We define the lagoon *size* to be the number s of sites in each patch. Thus we *exclude* ℓ-perimeter sites with $\ell \le \ell_0$ from contributing to the lagoon size [for illustration, see Figs. 3(e)–3(f)].

The sites where glove ℓ_0 "touches itself" identify a "neck" of width $w = 2\ell_0$ [46] — see Figs. 3(a)–3(c).

Roughly speaking, w is the diameter of the smallest disk that cannot penetrate into the lagoon. Using this "definition," we obtain the neck width $w = 2\ell_0 = 2$ for all the objects in Figs. 3(a)–3(c).

Even for a point set which is not connected — in contrast to the cluster types considered in this paper (DLA, PH, IP) — "lagoons" are still a meaningful concept. They identify volumes in space that are not accessible from the "exterior" by balls of diameter $> w$, where w is the neck width of the lagoon.

B. Lagoon-size distribution $N_M(s)$

We now analyze the number $N_M(w,s)$ of lagoons with size s and neck width w for discretized *off-lattice* DLA of mass M, where we take M to be the number of occupied lattice sites of the discretized cluster. First, we compute the number $N_M(s)$ of lagoons of size s by summing $N_M(w,s)$ over all neck widths w, i.e.,

$$N_M(s) \equiv \sum_w N_M(w,s). \tag{4.1}$$

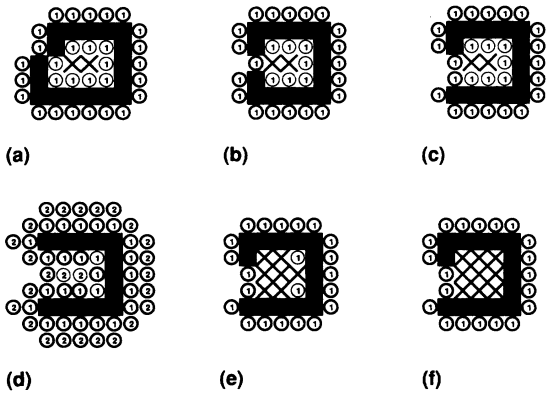

FIG. 3. (a), (b), (c) Small lagoons with openings of different sizes. The 1-gloves [boldface symbols ①] cannot penetrate into these openings. A lagoon can be identified by the vacant sites (×) left inside once its opening is "sealed." Some ℓ-perimeter sites [①] — those neighboring previous gloves or the object itself — are retained in the construction process for technical reasons concerning the next-nearest-neighbor connectivity of the discretized off-lattice DLA clusters. The lagoon area s is given by the number of sites left vacant, here $s = 2$. In all cases (a)–(c), the lagoon is sealed by the ℓ_0 = 1-glove. Thus, the neck width according to the definition in Sec. IV A is given by $w = 2\ell_0 = 2$. (d) The opening is so large that no lagoon is formed. (e),(f) A more reasonable definition of the *total lagoon size* is obtained, if perimeter sites with $\ell < \ell_0$ inside the lagoon are removed. To this end, we (1) identify the perimeter sites of the vacant lagoon sites. (e) In step (2), those perimeter sites, which (i) do not belong to the object itself, (ii) do not separate two lagoons, and (iii) have no neighbor with larger ℓ-value than themselves are freed. (f) The removal process [steps (1) and (2)] is repeated as long as additional sites are freed. All vacant and freed sites associated with the original smaller patch now contribute to the *total lagoon size* $\tilde{s}$; here $\tilde{s} = 9$.

In order to derive the scaling behavior of $N_M(s)$, we consider a covering of the fractal with boxes of linear size ϵ. The number of boxes necessary for such a covering is $\sim \epsilon^{-d_f}$. If ϵ is now increased to $\epsilon + d\epsilon$, then only $\sim (\epsilon + d\epsilon)^{-d_f}$ boxes are required to overlay all sites of the fractal. The difference in the total area covered by boxes is accounted for by voids or lagoons of linear size ϵ. Thus we obtain for the number of voids and lagoons $N(\epsilon)$ the expression

$$N(\epsilon)d\epsilon \sim \left(\frac{d}{d\epsilon}\epsilon^{-d_f}\right) d\epsilon \sim \epsilon^{-d_f-1}d\epsilon. \tag{4.2}$$

Earlier studies of DLA [47] indicate that DLA is a treelike object and consequently the occurrence of loops leading to voids in the cluster structure is negligible. Thus, for DLA, $N(\epsilon)$ should be considered to be the number of lagoons of linear size ϵ. Because ϵ and s are related by $\epsilon \sim s^{1/2}$, we obtain the distribution $N_M(s)$ of lagoon sizes by changing variables,

$$N_M(s) = N(\epsilon)\frac{d\epsilon}{ds} \sim s^{-\tau_s}, \tag{4.3}$$

where $\tau_s = d_f/2 + 1$.

In Fig. 4(a) we show the normalized distribution

$$n_M(s) \equiv N_M(s) \Big/ \sum_s N_M(s). \tag{4.4}$$

The data are obtained by averaging over 21 DLA clusters with masses M = 10 000, 40 000, and 120 000. Over almost three decades of lagoon sizes, with increasing range for larger clusters, we find power-law behavior,

$$n_M(s) \sim s^{-\tau_s}, \tag{4.5a}$$

with an exponent

$$\tau_s = 1.84 \pm 0.03. \tag{4.5b}$$

To ensure that our result (4.5b) does not depend in a significant manner on the specific definition of the lagoon size s, we will here briefly study the size distribution of lagoons as a function of the *total lagoon size* $\tilde{s}$. The total lagoon size $\tilde{s}$ *includes* the ℓ-perimeter sites situated "between" the vacant lagoon patch and the fractal object. We refer the reader to Figs. 3(e,f) for illustration of the concept of total lagoon size. Note that for each lagoon, we have $\tilde{s} \geq s$.

In analogy to $N_M(s,w)$, we consider $\tilde{N}(\tilde{s},w)$, the average number of lagoons of "total size" $\tilde{s}$ and neck width w in a DLA cluster of mass M. The inset of Fig. 4(a) presents the normalized distribution, defined in analogy to Eq. (4.4),

$$\tilde{n}_M(\tilde{s}) \equiv \tilde{N}_M(\tilde{s}) \Big/ \sum_{\tilde{s}} \tilde{N}_M(\tilde{s}), \tag{4.6}$$

where

$$\tilde{N}_M(\tilde{s}) \equiv \sum_w \tilde{N}_M(w,\tilde{s}), \tag{4.7}$$

analogous to Eq. (4.1). From the figure, we see that $\tilde{n}_M(\tilde{s})$ is very similar to $n_M(s)$. In particular, $\tilde{n}_M(\tilde{s})$ displays power-law behavior in the range $10 < \tilde{s} < 2000$,

$$\tilde{n}_M(\tilde{s}) \sim s^{-\tilde{\tau}_s}. \tag{4.8a}$$

Finite cluster sizes cause the breakdown of power-law behavior for large $\tilde{s}$, but the range over which the power-law applies increases with cluster mass M.

We find the exponent $\tilde{\tau}_s$ of the power law (4.8a) to be

$$\tilde{\tau}_s = 1.83 \pm 0.06. \tag{4.8b}$$

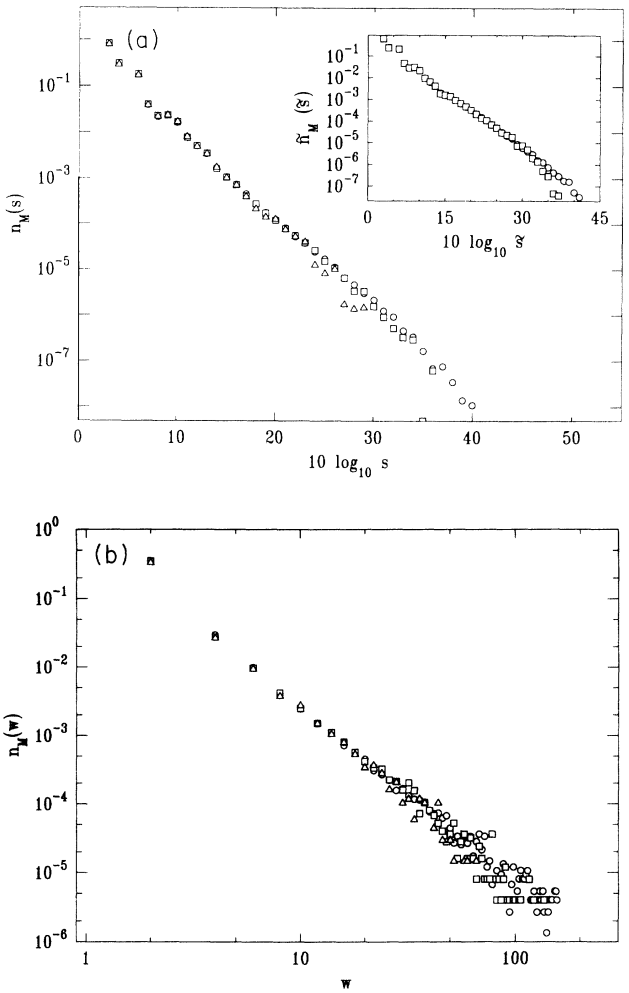

FIG. 4. (a) Lagoon-size distribution of DLA. We plot the normalized number of lagoons $n_M(s)$ vs their size $10\log_{10} s$. Data are obtained from 21 off-lattice 2D DLA clusters with masses $M = 120\,000$ (○), $M = 40\,000$ (□), and $M = 10\,000$ (△). The exponent characterizing the power-law part $10 < s < 10\,000$ is $\tau_s = 1.84 \pm 0.03$. The inset shows the distribution $\tilde{n}_M(\tilde{s})$ as a function of $10\log_{10} \tilde{s}$ for $M = 40\,000$ (○) and $M = 10\,000$ (□). From the slope, we obtain an exponent $\tilde{\tau}_s = 1.83 \pm 0.06$. From Eq. (4.3) we expect that in both cases $\tau = 1 + d_f/2 \approx 1.855$. (b) Neck size distribution $n_M(w)$ of DLA. For the masses $M = 120\,000$ (○), $M = 40\,000$ (□), and $M = 10\,000$ (△) the normalized distribution $n_M(w)$ is displayed. From the slope we obtain $\tau_w = 2.6 \pm 0.25$. The theoretical value is $\tau_w = d_f + 1 \approx 2.71$.

To within the accuracy of our simulations, $\tilde{\tau}_s$ equals τ_s.

From our calculations and the theoretical prediction in Eq. (4.3) we conclude that the lagoon-size distribution of DLA is characterized by its fractal dimension and no effect of necks is visible. In this light, we use the lagoon-size distribution as an independent measure of the fractal dimension of DLA. From τ_s via Eq. (4.3) we obtain an estimate for $d_f = 2(\tau_s - 1) = 1.68 \pm 0.06$; and similarly from the power-law behavior of $\tilde{n}_M(\tilde{s})$ we conclude $d_f = 1.66 \pm 0.12$.

C. Joint distribution $N_M(s,w)$ of lagoon size and neck width

We now discuss the joint distribution $N_M(s,w)$. The inset of Fig. 5 shows the behavior of $N_M(s,w)$ in a contour plot. We observe that most of the lagoons in DLA have small neck widths w. In particular, we observe that the distribution shows a pronounced vertical "ridge" that singles out a value for w for every given lagoon size s and that a significant number of large lagoons display small neck widths. Thus we are led to consider "cuts" through the distribution $N_M(s,w)$ considering s as parameter and w as independent variable. Let $n_M(s,w)$ be the number of lagoons of size s in clusters of mass M and normalized with respect to w,

$$n_M(s,w) \equiv N_M(s,w) \Big/ \sum_{w'} N_M(s,w'). \tag{4.9}$$

Figure 5 displays $n_M(s,w)$ for several values of s as a function of the rescaled neck width $w/s^{0.5}$. The ordinate is $n_M(s,w)s^{0.5}$, where the factor $s^{0.5}$ is included to preserve the normalization of $n_M(s,w)$. We obtain a data collapse which implies that the neck width scales as $s^{0.5}$, the linear extension of the lagoon [48]. We estimate the error of the exponent to be 0.05. However, the location of the maximum of the distributions $n_M(s,w)$ is at quite small values of w (e.g., $w \approx 10$ for $s = 2\,500$). Moreover, the size distribution of lagoons is maximal at small s, so we also expect the distribution of neck widths to be maximal for small w.

D. Neck-width distribution $N_M(w)$

A study of the normalized distribution $n_M(w)$ of necks as a function of their width w, in analogy to the normalized lagoon-size distribution $n_M(s)$, confirms that the distribution is maximal for small w. The distribution $n_M(w)$ is obtained from $N_M(s,w)$ using the one-to-one correspondence of neck widths and lagoons, i.e.,

$$n_M(w) \equiv \sum_s N_M(s,w) \Big/ \sum_{s,w} N_M(s,w). \tag{4.10}$$

Figure 4(b) shows that $n_M(w)$ can be approximated by a power law,

$$n_M(w) \sim w^{-\tau_w}, \tag{4.11a}$$

where

$$\tau_w = 2.6 \pm 0.25. \tag{4.11b}$$

To interpret this result, we employ the relation between most probable neck width and lagoon size $w \sim s^{1/2}$. Then we obtain the distribution $n_M(w)$ by a change of variables in $n_M(s)$ [Eq. (4.3)], i.e.,

$$n_M(w) = n_M(s)\frac{ds}{dw} \sim w^{-\tau_w}, \tag{4.12a}$$

where

$$\tau_w = d_f + 1. \tag{4.12b}$$

From Eq. (4.12a) we obtain

$$d_f = \tau_w - 1 = 1.6 \pm 0.25 \tag{4.12c}$$

for the fractal dimension of DLA.

We note that our results on the lagoon-size and neck-width distributions are consistent with a self-similar picture of DLA, in which the average neck width scales proportional to the linear size of the lagoons [19,20]. Our results support the finding [20,26] that the ratio of average fjord width to depth approaches a constant for large fjords (fjords are the regions between two major branches of a DLA cluster).

However, for two reasons our results are also consistent with a hierarchical "void-neck" picture for the structure of DLA [21,23,49] — which consists of a succession of increasingly larger, self-similar lagoons connected by narrow necks scaling *weaker than proportional* to the lagoon depth. (i) We find that even very large lagoons display very narrow necks and that the most probable neck width is located at rather small values of w. (ii) The void-neck picture [23] has been devised to provide an explanation for the peculiar scaling behavior of the smallest growth probability $p_{\min}$ of DLA. However, to explain the scaling behavior of $p_{\min}$, it suffices if one "void-neck" configuration exists per cluster at whose bottom $p_{\min}$ resides. The existence of such a configuration is still possible in the light of the presented results.

E. The accumulated lagoon area $A_M(w)$

One particular "moment" of the distribution $N_M(w,s)$ can be attributed an immediate geometric meaning. Define $A_M(w)$ to be the average accumulated size of all lagoons with neck width smaller than or equal to a given w,

$$A_M(w) \equiv \sum_{w'=0}^{w} \sum_{s=1}^{\infty} sN_M(s,w'). \tag{4.13}$$

Operationally, $A_M(w)$ is the mean area that a particle of linear extension w is affected by when it approaches the object. In analogy to Eq. (3.3a) for the ℓ-perimeter, we

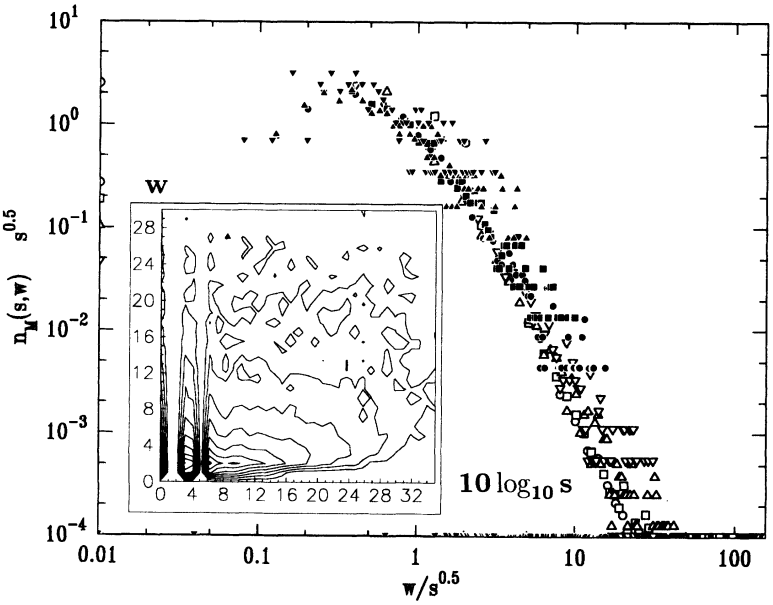

FIG. 5. Distribution $n_M(s,w)$ for $M = 120\,000$. $n_M(s,w)$ is obtained by normalizing the histogram $N_M(s,w)$ with respect to summation over w. On the abscissa we have plotted the rescaled neck width $w/s^{0.5}$, whereas the ordinate displays $n_M(s,w)s^{0.5}$. The factor $s^{0.5}$ is included to preserve the normalization of the distribution. From the quality of the scaling for different values of the exponent α used to rescale the neck width w/s^{α} we estimate $\alpha \approx 0.5 \pm 0.05$. Data are averaged over 21 off-lattice 2D DLA clusters. Different symbols denote different lagoon sizes: $s = 1$ (○), 3 (□), 10 (△), 25 (▽), 100 (•), 250 (■), 1000 (▲), 2500 (▼). We conclude that the width of a neck associated with a lagoon scales as a typical linear extension of the lagoon. Inset: Contour plot of $N_M(s,w)$. The ordinate is $10 \log_{10} s$ and the abscissa the linear neck width w; here, $M = 120\,000$. The spacings between successive levels are factors of 10, the lowest level is 0.1. The inset shows that even for large lagoons the most probable neck width is small.

expect that

$$A_M(w) \sim a(w)M \qquad (w \ll w_\times). \tag{4.14}$$

Here, $a(w)$ describes the w dependence of $A_M(w)$ and $w_\times$ is a crossover neck width which we expect to be proportional to the span L of the cluster (although considerably smaller than L).

For large $w \gg w_\times$, when the necks of all lagoons have been detected, $A_M(w)$ saturates to a w-independent value $A_M(\infty)$, which still depends on the mass of the aggregate. The dominant contribution to $A_M(\infty)$ arises from lagoons with a linear extension $\sim L$. Thus $A_M(\infty)$ scales as L^2,

$$A_M(\infty) \sim L^2 \sim M^{2/d_f} \qquad (w \gg w_\times). \tag{4.15}$$

We next make a scaling ansatz to describe both the M and the w dependence of $A_M(w)$. The scaling variable is chosen to be $u \equiv w/M^{1/d_f}$, since we expect M^{1/d_f} to be the relevant length scale in the problem. We obtain

$$A_M(w) \sim M^{2/d_f} h(w/M^{1/d_f}), \tag{4.16a}$$

where

$$h(u) \sim \begin{cases} u^{2-d_f}, & u \to 0 \\ \text{const}, & u \to \infty. \end{cases} \tag{4.16b}$$

Power-law behavior of $h(u)$ for small u is necessary to recover $A_M(w) \sim M$ for small w and implies that $A_M(w)$, considered for fixed M, scales as w^{2-d_f}.

In Fig. 6 we present a plot of $h(u) = A_M(w)/M^{2/1.7}$ vs $u = w/M^{1/1.7}$. For small values of the scaling variable u, we observe power-law behavior characterized by an exponent of 0.32 ± 0.02 corresponding to $d_f = 1.68 \pm 0.02$. Since the slope measures the codimension $2-d_f$, our 6.3% error in the slope translates to a 1.2% error in the value of d_f. For large values of u, $h(u)$ saturates and approaches a constant, as expected (4.15). Again, we see that only the self-similarity of DLA is needed to explain the scaling properties of $A_M(w)$ and that no effect of necks persists asymptotically.

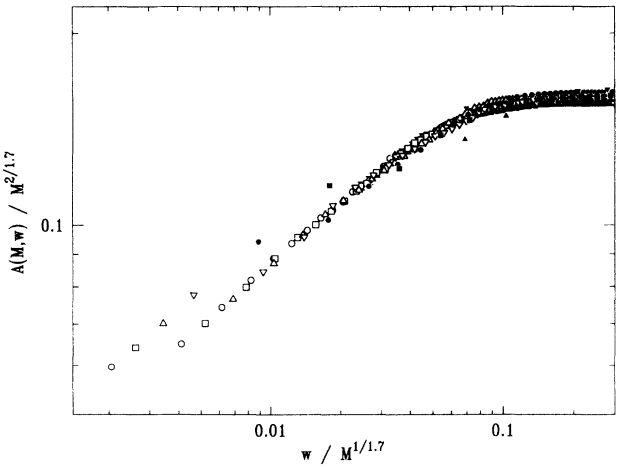

FIG. 6. Scaling function for the accumulated lagoon area $h(u) \equiv A_M(w)/M^{2/1.7}$ vs $u = w/M^{1/1.7}$. Data are obtained from 21 off-lattice DLA clusters in the mass range 300–120 000: 300 (▼), 1000 (▲), 3 000 (■), 10 000 (•), 30 000 (▽), 50 000 (△), 80 000 (□), and 120 000 (○). Next-nearest-neighbor connectivity is used in the glove determination. The labels on the ordinate extend from 0.06 to 0.2.

V. DISCUSSION AND CONCLUSION

We have introduced an algorithm to study properties of 2D fractal objects. We have studied the ℓ-perimeter and the ℓ-glove of DLA and, in the appendices, of the percolation hull and invasion percolation—as well as the lagoon-size distribution $N_M(s,w)$ and the neck-width distribution $N_M(w)$ of DLA.

For the ℓ-perimeter and the ℓ-glove we find scaling relations with interesting properties.

(i) The scaling relations for the ℓ-perimeter can be used for the determination of the fractal dimension of a wide class of fractal growth phenomena. We have used the scaling of the ℓ-perimeter successfully to numerically evaluate the fractal dimension of DLA, PH, and IP. We have confirmed that our method also works for the Sierpiński gasket, for which we can give an exact solution for the scaling function for ℓ-perimeter and ℓ-glove (Appendix A).

(ii) The scaling plots for the ℓ-gloves are sensitive to peculiarities in the scaling behavior of the fractal surface. In particular, a breakdown of the proposed scaling form for the ℓ-gloves occurs if the fractal dimension of the ℓ-gloves depends on the index ℓ. For example, the crossover from hull dimension to accessible perimeter dimension of conventional percolation as a function of ℓ is apparent in a scaling plot of $G(M,\ell)$ for PH. Using ℓ-gloves, we find that the hull dimension of IP *with trapping* is distinct from the fractal dimension of the IP cluster and very close if not equal to the value of $d_h = 7/4$ for conventional percolation. The accessible perimeter of IP with trapping ($\ell > 1$) is indistinguishable from the accessible perimeter of IP without trapping. We find that its fractal dimension agrees with the value for conventional percolation $d_a \approx 4/3$ to within our error bars.

In our analysis of 2D off-lattice DLA in circular geometry, we obtain six estimates for d_f from the scaling relations for the ℓ-perimeter (Sec. III B) and the ℓ-glove (Sec. III C), from the lagoon-size distributions $n_M(s)$ and $n_M(\tilde{s})$ (Sec. IV), from the neck-width distributions (Sec. IV) and from the accumulated lagoon area (Sec. IV E). We obtain a weighted average [50] of $d_f = 1.697 \pm 0.015$. Previous studies on 2D off-lattice DLA obtain $d_f = 1.715(\pm 0.004)$ [44] from the scaling of the radius of gyration of DLA with cluster mass. Our result disagrees with the value $d_f = 1.6 \pm 0.02$ [51] found using a generalized box-counting procedure.

Like a recent analysis of the branching properties of DLA [52], the analysis of the lagoon-size and neck-width distributions in 2D off-lattice DLA is consistent with an overall self-similar picture of DLA [20,19]. However, certain features of the growth probability distribution (GPD) of DLA [14,23–25] cannot be understood in the framework of a purely self-similar structure of DLA.

The void-neck model [21,23] explicitly takes into account fluctuations around a self-similar structure in the

form of side branches reaching far into the cluster fjords. Since in principle the presence of one void-neck configuration per cluster suffices to explain some of the peculiarities of the GPD of DLA, our analysis does not preclude the void-neck model. However, in the light of the result that the typical neck width is proportional to a typical measure for the linear size of a lagoon, it seems unlikely that the void-neck model can serve as model for the typical structure of DLA. The question of what to put in its place remains open.

ACKNOWLEDGMENTS

We would like to thank D. Avnir, A.-L. Barabási, S. Buldyrev, A. Bunde, A. Coniglio, M. Gyure, H. J. Herrmann, G. Huber, P. Ossadnik, S. Sastry, F. Sciortino, T. Vicsek, and M. Wolf for useful discussions. J. Lee made valuable comments on the manuscript. Paul Meakin kindly provided off-lattice DLA clusters for our study. S.S. appreciates the help of R. Putnam with computational aspects of this work. Finally, we gratefully acknowledge financial support by the NSF.

APPENDIX A: ℓ-PERIMETER AND ℓ-GLOVE FOR THE SIERPIŃSKI GASKET

In this appendix we demonstrate the scaling behavior of the ℓ-glove and the ℓ-perimeter for the Sierpiński gasket, an elementary deterministic fractal. In Figs. 7(a)–7(d) we show the first four construction steps of the Sierpiński gasket. Here, we use continuum analogues of the discrete quantities introduced in Secs. II, III B, and III C. The length L of one of the sides of the gasket

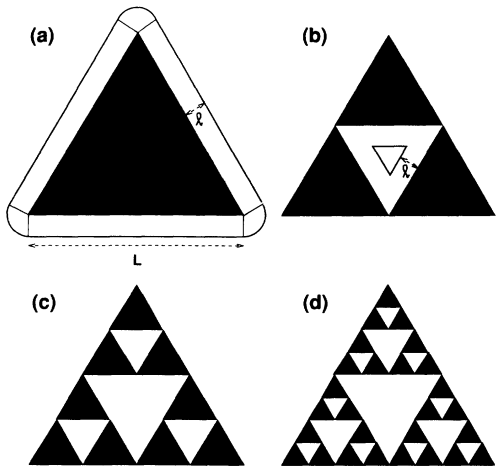

FIG. 7. (a)–(d) The first four construction stages of a Sierpiński gasket of base length L. In (a) we also indicate the ℓ-glove, consisting only of points accessible from the exterior, which here is the perimeter of the $r = \ell$-neighborhood of the compact equilateral triangle. In the first iteration step, shown in (b), we obtain one internal void with height half that of the original triangle. In addition to the ℓ-glove, the ℓ-perimeter comprises also contributions from internal voids if ℓ is so small that these voids are not completely filled in.

corresponds to the "overall linear extension" of the investigated fractal. The Euclidean distance ℓ to the sides of the gasket and its internal voids corresponds to the chemical distance as introduced in Sec. II.

The ℓ-glove is constituted only of sites that are accessible from the exterior. Apparently, the length of the ℓ-glove $G(\ell)$ is simply the length of the perimeter of the object indicated in Fig. 7(a), which is the Minkowski sausage of a compact equilateral triangle. The length $G(\ell)$ follows from elementary geometric considerations as the sum of the length of the linear and the circular segments of the perimeter,

$$G(\ell) = 3L + 2\pi\ell. \tag{A1}$$

We divide by ℓ and obtain the ratio $G(\ell)/\ell$,

$$\frac{G(\ell)}{\ell} = 3\left(\frac{\ell}{L}\right)^{-1} + 2\pi, \tag{A2}$$

where we have rewritten the right hand side of the equation as a function of the "scaling variable" ℓ/L. The structure of Eq. (A2) is the proposed scaling form (3.10a). In particular, for constant L, the singularity as $\ell \to 0$ is characterized by an exponent -1, corresponding to the "fractal" dimension $-(-1) = 1$ of the ℓ-glove (here a one-dimensional object), whereas for large ℓ the ratio G/ℓ approaches 2π, the ratio of perimeter to radius of a circle.

For the present example it is also possible to calculate an analytic expression for the scaling function $P(\ell)/\ell$ of the ℓ-perimeter. We consider the iterative construction of a Sierpińksi gasket of fixed base length L. In the zeroth construction step, we do not have any internal voids of the gasket contributing to $P(\ell)$ and expression (A2) with $G(\ell) = P(\ell)$ applies. In the first iteration — indicated by the superscript (1) — we must add the contribution arising in the large central void [see Fig. 7(b)]. We obtain

$$P^{(1)}(\ell)/\ell = 3\frac{L}{\ell} + 2\pi + \begin{cases} 0 & \text{if } (\frac{3}{2}\frac{L}{\ell} - 6\sqrt{3}) < 0 \\ \frac{3}{2}\frac{L}{\ell} - 6\sqrt{3} & \text{otherwise.} \end{cases} \tag{A3}$$

In each generation, we must add the contribution from the newly generated internal voids. However, geometrical considerations show that for any given value of ℓ, we only pick up contributions if the height of a void added in the kth iteration exceeds ℓ by a factor of 3 or, equivalently,

$$\frac{3}{2^k}\frac{L}{\ell} - 6\sqrt{3} > 0. \tag{A4}$$

For simplicity, let us consider $\ell = \ell_k$, such that $3L/2^k\ell_k - 6\sqrt{3} = 0$; ℓ_k is one-third of the height of one of the internal equilateral triangular voids added in the kth iteration. The dimensionless fraction L/ℓ_k results to

$$\frac{L}{\ell_k} = 2^{k+1}\sqrt{3}. \tag{A5}$$

In each generation the base length of the voids is reduced by a factor of $1/2$ and their number is multiplied by 3. If we replace ℓ in Eq. (A3) by ℓ_k and perform k iterations,

we obtain a finite sum for the dimensionless ratio of ℓ_k-perimeter to ℓ_k,

$$P(\ell_k)/\ell_k = 3\frac{L}{\ell_k} + 2\pi + \sum_{i=1}^{k} 3^{(i-1)} \left(\frac{3}{2^i} \frac{L}{\ell_k} - 6\sqrt{3} \right). \quad \text{(A6)}$$

Since all contributions from iteration steps $k+1, k+2, \ldots$ vanish, the expression (A6) is exact for the fully grown fractal. In analogy to the case of the ℓ-glove, $P(\ell_k)$ is the perimeter of the Minkowski sausage, here of the fully grown fractal and generated by dilation of the Sierpiński gasket with disks of radius ℓ_k.

It is straightforward to perform the sum in Eq. (A6). Moreover, if we use (A5) to replace k then, after some algebra, we obtain, for all $k \geq 1$,

$$P(\ell_k)/\ell_k = 3\sqrt{3} \left(\frac{1}{2\sqrt{3}} \right)^{d_f} \left(\frac{\ell_k}{L} \right)^{-d_f} + 3\sqrt{3} + 2\pi. \quad \text{(A7)}$$

Here, $d_f = \log 3/\log 2$ is the fractal dimension of the Sierpiński gasket. We see a power-law singularity characterized by the exponent $-d_f$ for small ℓ_k. If ℓ is larger than ℓ_1, or one-third of the height of the central void, we must replace Eq. (A7) by the expression (A2) for the ℓ-glove. In fact, ℓ-glove and ℓ-perimeter are identical for large ℓ. Thus we recover the large ℓ behavior of (A2) and $P(\ell)/\ell = 2\pi$.

In conclusion, we have demonstrated that the scaling forms for ℓ-perimeter and ℓ-glove hold for the Sierpiński gasket. Not only do we recover the $\ell/L \to 0$ and $\ell/L \to \infty$ limits as predicted in Secs. III B and III C but also the form of the scaling function.

APPENDIX B: ℓ-PERIMETER AND ℓ-GLOVE FOR THE PERCOLATION HULL (PH)

In this appendix we discuss the results of applying the scaling relations for ℓ-perimeter and ℓ-glove to a random fractal, here the hull of percolation clusters. The fractal nature of the PH is established and their fractal dimension is known to be $d_h = 7/4$ exactly [29,31,53].

1. The ℓ-perimeter of the PH

We consider the hull of a percolation cluster as a subset of the set of percolation cluster sites. The hull can be obtained, e.g., by a "walk" around the cluster. To this end, imagine a pointer directed from a tail site T to a head site H, which are two nearest-neighbor sites on the square lattice. The tail site shall be located in the cluster hull while the head site shall be an external perimeter site.

(i) Now turn the pointer counterclockwise around T by an angle of $\pi/2$ so that its head points to a new site H'. The pointer's tip will encounter either another external perimeter site or a cluster site. (ii) If the new head site H' is a perimeter site, then we repeat step (i). If, otherwise, we hit a cluster site, then we move the tail of the pointer in one of two ways. (a) If the next-nearest-neighbor site S located "between" H and H' is a cluster site, then S becomes the new tail site and we restore H as head site. (b) If S is, however, a perimeter site, then S becomes the new head and H' the new tail site of the pointer.

We repeat steps (i) and (ii) until the pointer has found its way around the entire cluster and is back in its starting position. The sites visited by the tail of the pointer constitute the hull of the percolation cluster. The perimeter sites visited by its head constitute the external perimeter of the cluster. In Fig. 1, hull sites are marked by black squares. Reference [12] describes how to efficiently *generate* percolation hulls using the above described "walk" technique without having to grow the entire percolation cluster.

In Fig. 8(a) we present data for the ℓ-perimeter of PH. The scaling function is

$$f_h(u) \equiv P_h(M,\ell)/\ell, \quad \text{(B1)}$$

where $P_h(M,\ell)$ is the number of sites in the ℓ-perimeter of percolation hulls of mass M and $u \equiv \ell/M^{1/d_h}$ is the scaling variable defined in Eq. (3.7a). Data are obtained by averaging over 50 percolation hulls with $M = 50, \ldots, 50\,000$, disregarding hulls with span of more than 1000 lattice units. For small u, as predicted by relation (3.7a), we observe a power-law singularity characterized by an exponent of about -1.75 ± 0.03, in agreement with the fractal dimension of PH. For large u, $f_h(u)$ approaches the constant value 4, which is the ratio of perimeter sites to radius of a diamond-shaped object on the square lattice.

2. The ℓ-glove and accessible perimeter of the PH

We now study the ℓ-gloves of PH. We will see that the ℓ-gloves for $\ell > 1$ are characterized by a *different fractal dimension* than the PH itself. In this section we use the PH example to demonstrate the usefulness of the glove algorithm in detecting peculiarities in the scaling properties of the PH. When we modify our definition of ℓ-gloves slightly, then we can see that the fractal dimension of the 1-glove is different from that of the l-gloves, with $l > 1$, leading to a breakdown of the scaling relation (3.10a) for small ℓ.

To this end, consider the perimeter-walk procedure introduced in the preceding section. The pointer's tail visits all sites of the PH. Its tip visits only perimeter sites and on completion of the walk, it has visited all sites of the external perimeter of the cluster. For illustration of the external perimeter, see Fig. 9. Here and in Appendix C, we want to consider the external perimeter as 1-glove of the studied object. Higher-order ℓ-gloves are defined by iteration; i.e., the 2-glove is the external perimeter of the union of the object and its 1-glove, the 3-glove is the external perimeter of the union formed by the object itself, its 1-glove and its 2-glove, and so forth.

The main difference between this definition and the one used for the study of DLA is that sites which are only accessible through next-nearest-neighbor links are

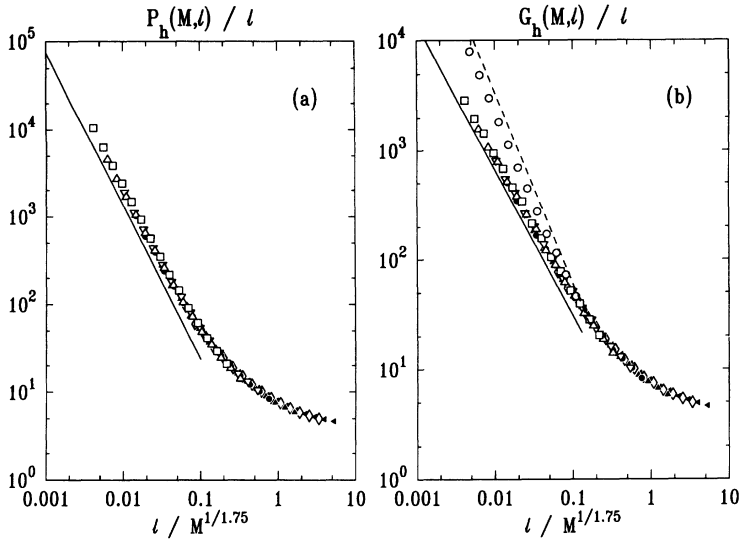

FIG. 8. (a) Scaling function $f_h(u) \equiv P_h(M,\ell)/\ell$ for the ℓ-perimeter of percolation hulls ($d_h = 7/4$), vs $u = \ell/M^{1/1.75}$. The solid line is a guide to the eye and has a slope of $-d_h = -7/4$, which reflects the slope for the expected asymptotic behavior of the scaling function for $u \to 0$. The displayed ℓ values are 2 (□), 3 (△), 5 (▽), 7 (•), 11 (■), 15 (▲), 23 (▼), 31 (◊), and 47 (◀). Data are averaged over 50 hulls with span $< 1\,000$ lattice units and $50 \leq M \leq 50\,000$. (b) Scaling function $g_h(u) \equiv G_h(M,\ell)/\ell$ vs $u = \ell/M^{1/1.75}$ for the ℓ-gloves of percolation hulls. The solid line has slope $-4/3$ which is the slope we expect for the scaling function $g_h(u)$ for small u. We find a slope of $1.33 \pm 0.04 \approx -d_a$ for the behavior of $g_h(u)$ as $u \to 0$. The displayed ℓ values and associated symbols are as in (a) with the addition that $\ell = 1$ is represented by ○. Note that the behavior of the $\ell = 1$ data points is different. As a function of u, they asymptotically lie on a line with slope equal to $-d_h = -7/4$ as indicated by the dashed line.

now *included* into the respective ℓ-glove [54]. However, the ℓ-glove remains a subset of the ℓ-perimeter and thus for fixed $\ell \ll \ell_\times$, $d_{\text{perimeter}} \geq d_{\text{glove}}$.

Before we turn attention to our calculations we must state some of the results obtained for the external and the accessible perimeter of percolation. The accessible perimeter consists of sites that are accessible from "infinity" by nearest-neighbor connections [cf. Fig. 1(a) for illustration]. The accessible perimeter of standard percolation clusters — which is identical to the accessible perimeter of PH — has been further constrained and has been investigated as a function of the radius r of a probe particle [30] approaching the perimeter from the cluster exterior. In particular, those perimeter sites have been considered which are connected to the exterior of the cluster by a path of minimum width $2r$ (for specific, small values of r). If r is increased from zero such that sites enclosed in "patches" only accessible through next-nearest-neighbor links are no longer accessible, then the fractal dimension of the perimeter sites accessible to the probe particle equals $d_a \approx 4/3$ and is independent of r.

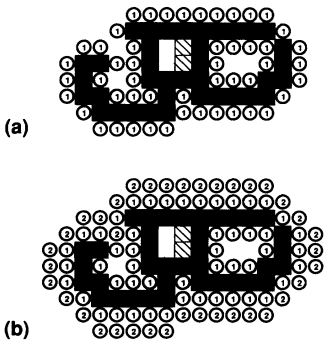

FIG. 9. To illustrate the algorithm used to determine the ℓ-gloves in the case of PH and IP, we use the same "object" and symbols as in Fig. 1. (a) 1-glove. The 1-glove is the set of external perimeter sites of the cluster, and is denoted by ①. (b) 1-glove and 2-glove. The 2-glove is the external perimeter of the set union of the object and its 1-glove sites. The 2-glove is denoted by ②.

The phenomenon that the fractal dimension of the perimeter is dependent on the radius of the probe particle is not restricted to lattice percolation [29,31], but extends to continuum percolation as well [55].

The ℓ-glove may be regarded as the *set of possible locations of centers* of diamond-shaped probe particles — in comparison to the set of 1-perimeter sites accessible to such particles. In both cases, the "radius" of the probe particle, here $r = \ell - 1$, limits the number of accessible locations, because a path of width $2r$ must exist that connects the accessible locations with the cluster exterior. For example, the 1-glove penetrates through next-nearest-neighbor links whereas the 2-glove does not. Therefore we expect that ℓ-gloves and accessible perimeters display similar scaling behavior.

In Fig. 8(b) we display a scaling plot of

$$g_h(u) \equiv G_h(M,\ell)/\ell \tag{B2}$$

vs $u \equiv \ell/M^{1/d_h}$. Here $G_h(M,\ell)$ is the number of sites in the ℓ-glove of PH, and M is the average mass of the PH used for obtaining the data. Because we generate

PH and not their accessible perimeters, we here use the scaling variable $\ell/M^{1/d_h}$ instead of $\ell/M_a^{1/d_a}$. Here M_a is the mass of the accessible part of the hull and d_a its fractal dimension.

Figure 8(b) confirms that the ℓ-gloves with $\ell > 1$ are described by the same fractal dimension $d_a \approx 4/3$ as the accessible perimeters, since the slope of $g_h(u)$ at small u is 1.33 ± 0.04.

As explained above, the external perimeter sites, a finite fraction of the perimeter sites of the percolation hull, become accessible if $\ell \leq 1$. The external perimeter has the same fractal dimension as the cluster hull [12], viz., $d_h = 7/4$, which is significantly different from $d_a \approx 4/3$ [30].

By comparison to the dashed line in Fig. 8(b) it is evident that $G_h(M, \ell = 1)$ — denoted by open circles — is characterized by a fractal dimension of $d_h = 7/4$ rather than $4/3$ as is $G_h(M, \ell > 1)$. Namely, since the number of sites in the 1-glove $G_h(M, \ell = 1)$ is proportional to the number M of sites in the PH, we find

$$G_h(M, \ell = 1)/\ell \sim M/1 \sim (1/L)^{-d_h}. \tag{B3}$$

The dashed line in Fig. 8(b) has a slope of $-d_h = -7/4$, which is in good agreement with the slope of $G_h(M, \ell = 1)/\ell$ as a function of $1/L$.

Different fractal dimensions for $\ell = 1$ and $\ell > 1$ had to be expected according to the exposition in the preceding paragraph.

Thus for $\ell = 1$, the scaling relation (3.10a) does *not* hold. PH provide an example in which the application of the glove algorithm reveals nontrivial scaling behavior of the fractal perimeter.

APPENDIX C: THE ℓ-PERIMETER AND ℓ-GLOVE OF INVASION PERCOLATION (IP)

Similar to PH, we consider IP as an example application of the glove algorithm. Comparatively little is known about the hull of IP with trapping. We find its fractal dimension to be close to d_h of conventional percolation (Appendix C 2).

1. The ℓ-perimeter of IP

Our IP clusters are grown starting from a central seed [27] on a square lattice and including the trapping rules of Ref. [10], namely, that once a loop has formed, no growth inside the loop can occur. Growth of the clusters is stopped as soon as their span, the largest extension in x or y direction, exceeds a given value L. References [10,11] find the fractal dimension of IP clusters to be $d_{\rm IP} \approx 1.82$.

We display data for the ℓ-perimeter of IP clusters with various L in Fig. 10(a). The scaling function $f_{\rm IP}(u)$ for the ℓ-perimeter $P_{\rm IP}(\ell, L)$ is plotted as a function of the scaling variable u; here u is the scaled chemical distance $u \equiv \ell/L$. The use of L in the scaling variable is equivalent to using $M^{1/d_{\rm IP}}$, since L is the linear extension of the cluster.

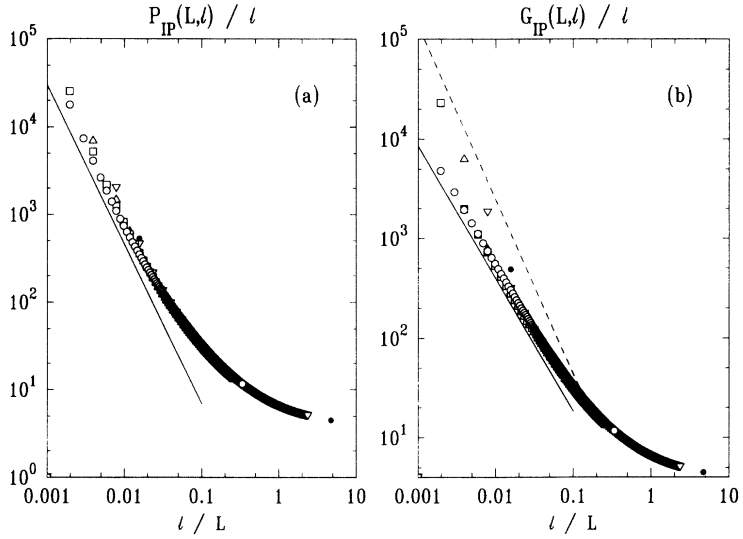

FIG. 10. (a) The scaling function $f_{\rm IP}(u) \equiv P_{\rm IP}(L, \ell)/\ell$ for the ℓ-perimeter of invasion percolation ($d_{\rm IP} \approx 1.82$), vs $u = \ell/L$. L denotes the span of the clusters and is equal to the linear size of the lattice on which the clusters are grown. The solid line is a guide to the eye and has a slope of 1.82. Different symbols indicate different values of L, $L = 1024$ (○), 512 (□), 256 (△), 128 (▽), 64 (•). The number of configurations averaged ranges from 10 for $L = 1\,000$ to 100 for $L = 64$. (b) Scaling function $g_h(u) \equiv G_h(M, \ell)/\ell$ vs $u = \ell/M^{1/1.75}$ for the ℓ-gloves of invasion percolation. The slope for small values of the scaling variable is $1.33 \pm 0.04 \approx d_a$. The solid line indicates a slope of 4/3. As in (a), different symbols denote different system size L; the same symbols have been used for the same system sizes. As in the percolation hull case, the behavior of the $\ell = 1$ data points is different. The dashed line indicates a slope of $= -1.75$ equal to the negative fractal dimension of *percolation hulls*. The accuracy of our data does not allow us to establish a distinct universality class for the hulls of IP clusters.

The solid line in Fig. 10 has a slope of 1.82 and is shown in order to compare the small u behavior of the scaling function $f_{\rm IP}(u)$ with the prediction in Sec. III B. We observe agreement of the behavior $f_{\rm IP}(u)$ with Eq. (3.7a) as the system size increases. However, the system size seems still too small for an accurate determination of $d_{\rm IP}$ from the scaling plot, since there are deviations from a straight line both for small ℓ/L and in the vicinity of the crossover to $f_{\rm IP}(u) \to$ const.

In both cases, PH and IP, we see that the small u behavior of the scaling functions $f_h(u)$ and $f_{\rm IP}(u)$ is consistent with the known values of $d_h = 7/4$ and $d_{\rm IP} \approx 1.82$, respectively. This observation supports our statement (Sec. III B) that scaling plots for the ℓ-perimeter allow for independent measurement of the fractal dimension of an object.

2. The ℓ-glove and the accessible perimeter of IP

We now consider the ℓ-gloves of clusters generated by the IP process with trapping. In particular, as in the PH case, the 1-glove will provide information about the hull of IP.

In Fig. 10(b) we display a scaling plot of $g_{\rm IP}(u) \equiv G_{\rm IP}(L,\ell)/\ell$ vs $u \equiv \ell/L$. Here $G_{\rm IP}(L,\ell)$ is the number of sites in the scheme A ℓ-glove of an IP cluster, and L is the linear extension of the lattice on which the IP cluster is grown. The lattice extension L plays the role of the length scale in analogy to M^{1/d_f} in the previous cases in the scaling variable $u = \ell/L$. The solid line in the figure has a slope of 4/3, which demonstrates that the small u behavior of $g_{\rm IP}(u)$ is consistent with a fractal dimension $d_a^{\rm IP} \approx 4/3$ of the accessible perimeter of IP clusters.

To better understand this result, we next describe the relation between the conventional percolation and the IP processes. If one does *not* apply a trapping rule during the invasion process, then *always* the site with the largest random number on the surface of the invasion percolation cluster is grown, even if it is enclosed in a loop. The resulting clusters are conjectured to fall into the universality class of standard percolation [10]. In fact, if we measure the ℓ-perimeter and the ℓ-glove of clusters grown without the trapping rule, we find that the fractal dimension of the ℓ-perimeter agrees well with the value expected from standard percolation $d_f = 91/48$ value and the ℓ-gloves display a dimension of $\approx 4/3$, the value expected from the scaling of the accessible perimeter of standard percolation (cf. Appendix B 2).

The application of the trapping rule changes the universality class such that the fractal dimension of IP clusters *with trapping*, $d_f^{\rm IP} \approx 1.82$, is smaller than the fractal dimension of standard percolation $= 91/48 \approx 1.89$. Since the trapping rule only excludes perimeter sites in the interior of the cluster from further growth, there is no change in the structure of the external surface of the cluster. In other words, if on the same lattice with the same distribution of random numbers, two IP clusters are grown — one with and the other without the trapping rule — then for each stage in the growth process of the cluster with trapping, there is a stage of the growth of the cluster without trapping with exactly the same geometric arrangement of the external cluster surface. Consequently, the fractal dimension of the accessible perimeter and the scaling behavior of the ℓ-gloves — $\ell > 1$ — are identical in both the IP and PH cases.

Just as in the PH case, we observe a breakdown of the scaling behavior (3.10a) for $\ell = 1$ in the case of IP with trapping. Here, $G_{\rm IP}(L, \ell = 1)$ — the number of sites in the $\ell = 1$-glove, corresponding to the data points of largest magnitude in each of the data sets shown in Fig. 10(b)] — display a different functional dependence on ℓ/L than $G_{\rm IP}(\ell, L)$ for $\ell > 1$.

The 1-glove can penetrate through diagonal openings. Therefore all 1-glove sites are nearest neighbors of the cluster hull. Conversely, all hull sites are nearest or next-nearest neighbor of at least one 1-glove site. Thus the number of 1-glove sites is asymptotically proportional to the number of hull sites. There is, however, no apparent reason why the hull of IP clusters *with trapping* should be in the same universality class as the hull of standard percolation. If the hull of IP clusters with trapping has a fractal dimension different from 7/4, then the difference must be very small, since the data displayed in Fig. 10(b) are consistent with the assumption that also the hull of IP clusters is characterized by $d_h = 7/4$. The consistency is evident from comparison of the data with the dashed line of slope $-1.75 = -d_h$.

We conclude that the hull of invasion percolation with trapping has a fractal dimension $d_h^{\rm IP} < 1.82 \approx d_{\rm IP}$ and close to $7/4 = d_h$, the hull dimension of conventional percolation.

[1] This observation is based on topological properties of fractals. All points of an idealized mathematical fractal belong to its boundary, so that each ϵ-neighborhood of any point of the fractal contains points of both the fractal and its complement, since otherwise one could find an ϵ-neighborhood entirely composed of fractal points, and its Hausdorff dimension would be equal to the dimension of the embedding space.

[2] *The Fractal Approach to Heterogeneous Chemistry*, edited by D. Avnir (Wiley, New York, 1989).

[3] *Fractals and Disordered Systems*, edited by A. Bunde and S. Havlin (Springer, New York, 1991); *Fractals in Science*, edited by A. Bunde and S. Havlin (Springer, New York, 1993).

[4] P. Meakin, in *Phase Transitions and Critical Phenomena*, edited by C. Domb and J. L. Lebowitz (Academic, Orlando, 1988), Vol. 12.

[5] J. Feder, *Fractals* (Pergamon, New York, 1988).

[6] *Fractals: Physical Origin and Properties*, Proceedings of the 1988 Erice Workshop on Fractals, edited by L.

Pietronero (Plenum Publishing Co., London, 1990).
[7] *Fractals in Physics: Essays in Honor of B. B. Mandelbrot*, edited by A. Aharony and J. Feder (North-Holland, Amsterdam, 1990).
[8] *Correlations and Connectivity: Geometric Aspects of Physics, Chemistry and Biology*, edited by H. E. Stanley and N. Ostrowsky (Kluwer Academic Publishers, Dordrecht, 1990).
[9] T. Vicsek, *Fractal Growth Phenomena*, 2nd ed. (World Scientific, Singapore, 1992).
[10] In this paper, we consider the original Lenormand model with trapping, i.e., no growth occurs inside "lakes" enclosed in loops of cluster sites. R. Lenormand, C. R. Acad. Sci., Ser. B **291**, 279 (1980); see also D. Wilkinson and J. F. Willemsen, J. Phys. A **16**, 3365 (1983).
[11] L. Furuberg, J. Feder, A. Aharony, and T. Jøssang, Phys. Rev. Lett. **61**, 2117 (1988).
[12] R. M. Ziff, P. T. Cummings, and G. Stell, J. Phys. A **17**, 3009 (1984).
[13] P. Meakin, H. E. Stanley, A. Coniglio, and T. A. Witten, Phys. Rev. A **32**, 2364 (1985); P. Meakin, A. Coniglio, H. E. Stanley, and T. A. Witten, *ibid.* **34**, 3325 (1986).
[14] J. Lee and H. E. Stanley, Phys. Rev. Lett. **62**, 2945 (1988).
[15] C. Amitrano, A. Coniglio, P. Meakin, and M. Zannetti, Phys. Rev. B **44**, 4974 (1991).
[16] C. J. G. Evertsz and B. B. Mandelbrot, Physica A **185**, 77 (1992); C. J. G. Evertsz, B. B. Mandelbrot, and L. Woog, Phys. Rev. A **45**, 5798 (1992).
[17] Recent progress embraces the fixed-scale transform: L. Pietronero, A. Erzan, and C. J. G. Evertsz, Physica A **151**, 207 (1988); A. Vespignani and L. Pietronero, *ibid.* **173**, 1 (1991); L. Pietronero, S. Sidoretti, and A. Vespignani, Fractals **1**, 41 (1993); R. De Angelis, M. Marsili, L. Pietronero, A. Vespignani, and H. J. Wiesmann, Europhys. Lett. **16**, 417 (1991); M. Di Stasio, L. Pietronero, A. Stella, and A. Vespignani, J. Phys. A (to be published).
[18] T. C. Halsey and M. Leibig, Phys. Rev. A **46**, 7793 (1992).
[19] B. B. Mandelbrot and T. Vicsek, J. Phys. A **20**, L377 (1989).
[20] A. Barabási and T. Vicsek, J. Phys. A **23**, L729 (1990).
[21] J. Lee, S. Havlin, H. E. Stanley, and J. Kiefer, Phys. Rev. A **42**, 4832 (1990).
[22] J. Lee, P. Alstrøm, and H. E. Stanley, Phys. Rev. A **39**, 6545 (1989).
[23] The scaling form of the minimum growth probability of 2D DLA has been found to be $\log p_{\min} \sim (\log M)^2$ [S. Schwarzer, J. Lee, A. Bunde, H. E. Roman, S. Havlin, and H. E. Stanley, Phys. Rev. Lett. **65**, 603 (1990)]. In contrast, for 3D DLA one finds $p_{\min} \sim M^{-\alpha}$ [S. Schwarzer, M. Wolf, S. Havlin, P. Meakin, and H. E. Stanley, Phys. Rev. A **46**, 3016 (1992)].
[24] B. B. Mandelbrot and C. J. G. Evertsz, Nature (London) **348**, 143 (1990).
[25] M. Wolf, Phys. Rev. E **47**, 1448 (1993).
[26] R. C. Ball and R. Blumenfeld, Phys. Rev. A **44**, 828 (1991).
[27] L. de Arcangelis and H. J. Herrmann, J. Phys. A **23**, L923 (1990).
[28] P. Pfeifer, in *Proceedings of the IUPAC Symposium*, edited by K. V. Unger, D. Behrens, and H. Kral (Elsevier, Amsterdam, 1987).
[29] A. Bunde and J. F. Gouyet, J. Phys. A **18**, L285 (1985).
[30] T. Grossman and A. Aharony, J. Phys. A **19**, L745 (1986); **20**, L1193 (1987).
[31] H. Saleur and B. Duplantier, Phys. Rev. Lett. **58**, 2325 (1987).
[32] E. P. Stoll and M. Kolb, Physica A **185**, 222 (1992).
[33] The authors of Ref. [56] report calculations for the void-size distributions of on-lattice DLA and other aggregation phenomena. However, their algorithm cannot identify almost closed loops as the glove algorithm can. Similarly, this type of topological information is lost in algorithms designed to determine the lacunarity of fractals (see, e.g., [57]).
[34] Algorithms of this type are also known as "burning" algorithms; one example is given in Ref. [58], other examples useful for binary image processing in [59].
[35] Z. Alexandrowicz, Phys. Lett. A **80**, 284 (1980); R. Pike and H. E. Stanley, J. Phys. A **10**, L169 (1981); S. Havlin and R. Nossal, *ibid.* **17**, L427 (1984).
[36] B. Dubuc, J. F. Quiniou, C. Roques-Carmes, C. Tricot, and S. W. Zucker, Phys. Rev. A **39**, 1500 (1989).
[37] F. Normant and C. Tricot, Phys. Rev. A **43**, 6518 (1991).
[38] P. Pfeifer and M. Obert, in *The Fractal Approach to Heterogeneous Chemistry*, edited by D. Avnir (Wiley, New York, 1989).
[39] J. Serra, *Image Analysis and Mathematical Morphology* (Academic Press, London, 1982).
[40] G. Borgefors, Comput. Vision Graphics Image Processing **27**, 321 (1984).
[41] H. E. Stanley, *Introduction to Phase Transitions and Critical Phenomena* (Oxford University Press, Oxford, 1971).
[42] Consider, e.g., the number of nearest neighbors to fractal sites ($\ell = 1$). This number depends on the lattice type used for discretization. However, it is proportional to the cluster mass, since the internal sites of a fractal (sites surrounded by fractal sites only) constitute — even asymptotically — only a fraction of its mass.
[43] R. C. Ball and R. M. Brady, J. Phys. A **18**, L809 (1985).
[44] S. Tolman and P. Meakin, Phys. Rev. A **40**, 428 (1989); Physica A **158**, 801 (1989). Measuring the radius of gyration of DLA as a function of the cluster mass, a value of $d_f = 1.715 \pm 0.004$ for 2D off-lattice DLA is obtained, where the error corresponds to the 95% confidence limit. Note that our errors are standard deviations.
[45] C. Amitrano, P. Meakin, and H. E. Stanley, Phys. Rev. A **40**, 1713 (1989).
[46] Operationally, we identify lagoons as connected patches of vacant sites. For each lagoon, we obtain the unique neck width $w = 2\ell_0$ by finding the largest value of ℓ on the perimeter of the patch of lagoon sites. Note that this recipe works in all cases shown in Figs. 3(a)–3(c), and is therefore more precise than the somewhat vague notion of "ℓ_0-glove touching itself."
[47] P. Meakin, I. Majid, S. Havlin, and H. E. Stanley, J. Phys. A **17**, L975 (1984).
[48] An analysis of the inertia tensor of the lagoons $I_{ik} \equiv (1/\tilde{s}) \sum_{j=1}^{\tilde{s}} \delta_{ik} r_j^2 - x_{j,i} x_{j,k}$ yields a linear dependence of the square root of its smaller eigenvalue (considered to be a measure for the lagoon "width") from the square root of its larger eigenvalue (a measure for the lagoon "length"). In other words, neither neck width nor any of the two inertia lengths of the lagoons indicate self-affine scaling of the lagoon area.

[49] J. Lee, S. Havlin, and H. E. Stanley, Phys. Rev. A **45**, 1035 (1992).
[50] J. R. Taylor, *An Introduction to Error Analysis* (University Science Books, Mill Valley, CA, 1982).
[51] F. Argoul, A. Arneodo, G. Grasseau, and H. L. Swinney, Phys. Rev. Lett. **61**, 2558 (1988).
[52] P. Ossadnik, Phys. Rev. A **45**, 1058 (1992).
[53] A. Coniglio, N. Jan, I. Majid, and H. E. Stanley, Phys. Rev. B **35**, 3617 (1987).
[54] Note that defining the ℓ-gloves as external perimeters implies that the number of sites in the ℓ-glove is always greater than or equal to the resulting number if the DLA ℓ-glove definition had been used. Thus the fractal dimension of the ℓ-glove measured by the procedure employed for the DLA case is always less than or equal to the fractal dimension resulting from the external perimeter procedure. Do our results for the DLA ℓ-gloves also hold for the external perimeter definition of the ℓ-glove? If we had applied the external perimeter definition of the ℓ-gloves to DLA, we would have found on the one hand that the fractal dimensions of the ℓ-gloves for fixed $\ell \ll \ell_\times$ are $\geq d_f$, since they must be greater than the fractal dimensions measured with the DLA procedure. On the other hand, the fractal dimension of an ℓ-glove cannot be larger than d_f. Thus we recover the result that $d_{\text{glove}} = d_f$. In conclusion, our results for the DLA ℓ-gloves also hold for the alternative definition used for the study of PH and IP.
[55] M. Kolb, Phys. Rev. A **41**, 5725 (1990).
[56] F. Ehrburger-Dolle, P. M. Mors, and R. Jullien, J. Colloid Interface Sci. **147**, 192 (1991).
[57] C. Allain and M. Cloitre, Phys. Rev. A **44**, 3552 (1991).
[58] H. J. Herrmann, D. C. Hong, and H. E. Stanley, J. Phys. A **17**, L261 (1984).
[59] R. Creutzburg, A. Mathias, and E. Ivanov, Physica A **185**, 56 (1992).